Materials Science Forum
ISSN: 1662-9752, Vol. 854, pp 112-117
doi:10.4028/www.scientific.net/MSF.854.112

Submitted: 2015-09-21
Accepted: 2015-11-17
Online: 2016-05-17

Cyclic Tension Test of AZ31 Magnesium Alloy at Elevated Temperature Realized in a Miniaturized Uniaxial Tensile Test Setup

Sebastian Suttner[1,a *] and Marion Merklein[1,b]

[1]Institute of Manufacturing Technology (LFT), Friedrich-Alexander-Universität Erlangen-Nürnberg, D-91058 Erlangen

[a]sebastian.suttner@fau.de, [b]marion.merklein@fau.de

Keywords: Magnesium alloy, characterization, cyclic testing, Bauschinger effect

Abstract. The use of new materials, e.g. aluminum and magnesium alloys, in the automotive and aviation sector is becoming increasingly important to reach the global aim of reduced emissions. Especially magnesium alloys with their low density offer great potential for lightweight design. However, magnesium alloys are almost exclusively formable at elevated temperatures. Therefore, material characterization methods need to be developed for determining the mechanical properties at elevated temperatures. In particular, cyclic tests at elevated temperatures are required to identify the isotropic-kinematic hardening behavior, which is important for numerically modeling the springback behavior. In this contribution, a characterization method for determining the cyclic behavior of the magnesium alloy AZ31B at an elevated temperature of 200 °C is presented. The setup consists of a miniaturized tensile specimen and stabilization plates to prevent buckling under compressive load. The temperature in the relevant area is introduced with the help of conductive heating. Moreover, the complex kinematic model according to Chaboche and Rousselier is identified, to map the transient hardening behavior of AZ31B after load reversal, which cannot be modeled with a single Bauschinger coefficient.

Introduction

The reduction of greenhouse gas emission is one main objective in the field of automotive industry. A decrease of CO_2 emission up to 30 % in cars is possible by replacing conventional materials with modern lightweight material systems [1]. Counterpart to this is the energy-consuming process of manufacturing lightweight materials as aluminum or magnesium alloys. However, Pflieger et al. [2] analyzed the break-even points for the Global Warming Potential (GWP) of aluminum and magnesium alloys to conventional steel. They declare that the break-even point to steel is reached at a mileage of 50000 kilometer for a car, if the weight saving is more than 30 % by replacing steel with lightweight materials. Complementary to this result, Behrens et al. [3] showed the potential of weight reduction by substituting a car hood made of steel with the same part made of magnesium. In case of the magnesium alloy part a weight reduction of 56 % is reachable. Since the formability of magnesium sheets at room temperature is limited, the ability of using magnesium in sheet metal forming is paired with a forming temperature above 150 to 300 °C [4]. With an increase of the forming temperature from 20 °C to 200 °C, Ullmann et al. [5] detected an improvement of the ductility of AZ31 around 38 % in case of the elongation to failure. Due to the hexagonal close-packed microstructure, magnesium alloy sheets exhibit supplemental a significant tension-compression asymmetry, which is mostly characterized in uniaxial tension and compression tests [6]. Various specimen geometries exist to realize a tension-compression test of magnesium alloy sheets from 53.5 x 23.0 mm² (length x width) as proposed by Hama et al. [7] to smaller specimen with 2.0 x 2.0 mm² as used by Schaub et al. [8]. Within this contribution, a modification of a miniaturized tensile test setup is presented to realize cyclic tension tests (tension-compression tests) of AZ31B at elevated temperatures up to 200 °C. Moreover, the isotropic-kinematic material behavior is investigated and the kinematic material model Chaboche-Rousselier [9] is identified.

Tension-compression Tests at Elevated Temperature

Material and Experimental Setup. In this study, tension-compression tests are carried out on AZ31B magnesium alloy with an initial sheet thickness of 1.0 mm at a process-oriented temperature of 200 °C. Miniaturized specimen are cut out in 0° to the rolling direction (R.D.) by laser cutting (TruLaser Cell 7020, Trumpf GmbH + Co. KG). The cross section of the measuring zone is set to 2 x 2 mm² (width x length). Due to the small measuring area, the knowledge of the grain size is important to estimate the appearance of size effects. Thus, the grain size of 5.32 ± 1.84 µm is measured by EBSD (Merlin Gemini II, Carl Zeiss AG). According to Gau et al. [10] size effects need to be considered, if the aspect ratio of sheet thickness t_0 to the average grain size is smaller than 10. In case of the investigated AZ31B magnesium alloy, the aspect ratio is calculated to 188. Moreover, in-plane size effects can occur, if the specimen width is minimized. The aspect ratio of specimen width w_0 to the average grain size is calculated to 376. Thus size effects are not expected to be significant. Tension-compression tests are realized in a universal testing machine (Z100, Zwick Gmbh & Co. KG) with a built-in tool and a conductive heating system as seen in Fig. 1.

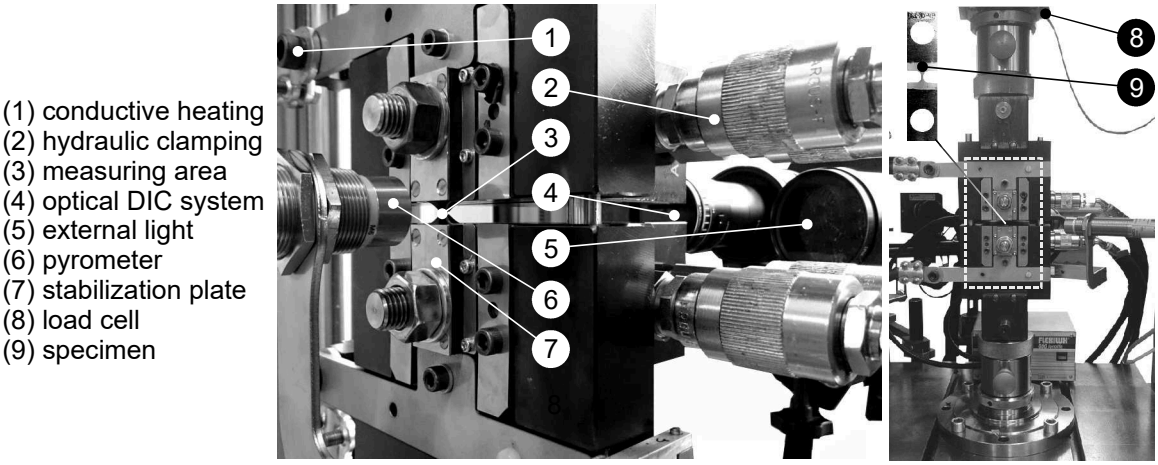

Fig. 1. Miniaturized tensile test setup with conductive heating and optical measurement system

The introduced temperature is regulated via a pyrometer, which is adjusted in the measuring area of the specimen. Due to the good thermal conduction of AZ31B, the test setup presented by Schaub et al. [8] is modified to achieve a constant temperature up to 200 °C for AZ31B. Therefore, the connection components for conductive heating are adjusted to reduce the electric resistance. The setup consists of an adjustable load cell to measure the tensile force F_x in the x-direction. The specimen is clamped in the center of the tool by a hydraulic clamping system with a maximum clamping pressure of 40 MPa. Additionally, stabilization plates are mounted to protect the specimen from buckling during compressive loading. Local strains are detected with an optical DIC system (ARAMIS, GOM mbH). Therefore, a fine stochastic pattern is sprayed via airbrush as seen in Fig. 2.

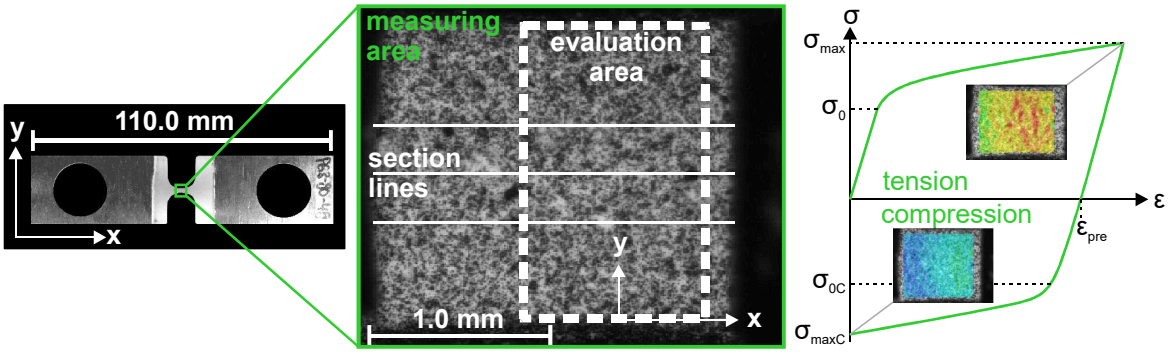

Fig. 2. Miniaturized tensile specimen with measuring area and principal of stress vs. strain curve

Concerning a small effective range and the conditional accessibility of clip gauge systems, the optical measuring system has the advantage of a detailed detection of local strains on small cross sections. For the determination of the average strains ε_x and ε_y, an evaluation area of 1 x 2 mm² is chosen centered around the maximum column of the local strains. The averaged strain distribution is investigated for three section lines with a section length l_x defined in the center of the specimen. The tensile tests are performed with a strain rate of 0.01 1/s and three trials (N = 3) for each configuration. To investigate the kinematic hardening behavior of AZ31B under cyclic loading, a test series with first loading under tension to three levels of pre-strain is carried out. The average pre-strains ε_{pre} are calculated in the evaluation area according to the equivalent strain of von Mises. Cyclic stress vs. strain curves include a positive (tension) and a negative (compression) stress zone as exemplarily shown in Fig. 2. Mechanical characteristics in the cyclic stress vs. strain curve are the beginning of plastic yielding after first loading σ_0, the maximum yield stress σ_{max} at a defined level of pre-straining ε_{pre}, the subsequent beginning of plastic yielding after load reversal σ_{0C} and the maximum yield stress σ_{maxC} under compression after a complete reversal of the pre-strain.

Experimental Results and Limitation of Pre-straining. Cyclic tests are carried out to characterize the isotropic-kinematic material behavior, which leads to a translation of the yield surface away from the center of the stress space. A simple alternative for modeling this translation is the description with one single parameter, e.g. the Bauschinger coefficient α. The parameter α is defined as the ratio of the subsequent beginning of plastic yielding σ_{0C} characterized at a plastic strain of 0.002 after load reversal to the maximum introduced stress σ_{max}. The experimental cyclic stress vs. strain curves and the identified Bauschinger coefficient of AZ31B for a temperature of 200 °C and three different levels of pre-strain are shown in Fig. 3.

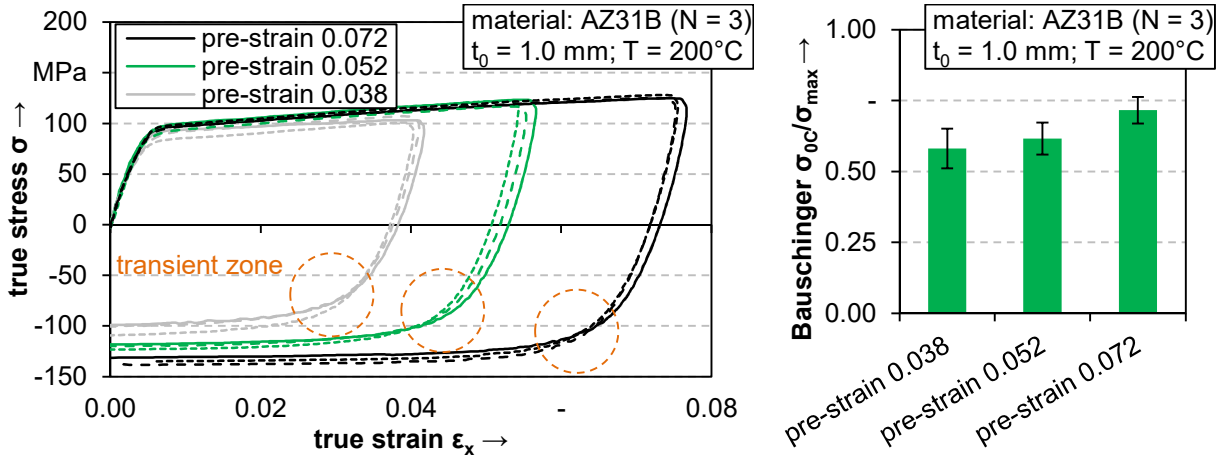

Fig. 3. Stress vs. strain curves of AZ31B at 200 °C (left) and Bauschinger coefficient σ_{0C}/σ_{max} (right)

In Fig. 3 the experimental results with the average pre-strains of 0.038 ± 0.001, 0.052 ± 0.001 and 0.072 ± 0.001 are shown. Straining leads to an increase of the yield stress under uniaxial tension with subsequent unloading at a defined pre-strain until reloading under compression is introduced. Moreover, reloading under compression firstly induces an elastic material behavior as far as a transient zone occurs, which marks the transition of the elastic to the plastic material behavior. The Bauschinger coefficient is increasing with rising pre-strain proportional to the subsequent beginning of plastic yielding. In case of a small pre-strain level of 0.038 the Bauschinger coefficient reaches a value of 0.581 ± 0.070, which indicates a significant Bauschinger effect on first view. Regarding the stress vs. strain curves, the transient zone and the chosen point of subsequent yielding at 0.002 plastic strain after load reversal, the influence of the transient zone on the determined Bauschinger coefficient leads to inaccurate values for the kinematic hardening behavior. The transient zone complicates the identification of the kinematic hardening behavior with only one specific Bauschinger coefficient and affirmed the need for a more complex material model.

Continuative, in the context of cyclic testing it is important that the strain distribution during tensile pre-straining shows the same profile as under subsequent compressive loading. This is an indication for an evenly strain hardening behavior during cyclic loading, which is important for the characterization of the kinematic hardening behavior. A shift of the straining position between tensile pre-strain and subsequent compressive straining leads to a falsification of the results and a monotonic loading behavior of partial areas in place of a cyclic loading. This means, the material experiences a monotonic load under tension or compression at different positions in the measuring area, not a cyclic load, which is required for characterizing the isotropic-kinematic material behavior. In Fig. 4, the strain distribution for the investigated maximum tension and compression load and the average strain distribution ε_x vs. section length l_x of the measuring area are shown.

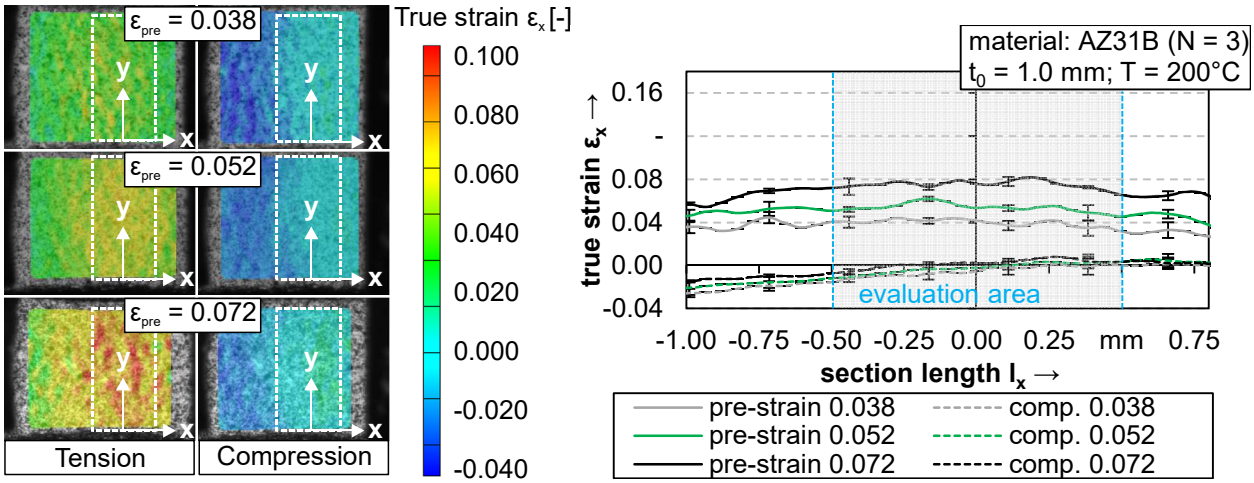

Fig. 4. Evolution of true strain ε_x in loading direction and strain distribution of AZ31B under tensile and compressive load at 200 °C for three levels of pre-straining

The results show an increase of the strain level with rising level of pre-strain at σ_{max} (tension) and an almost constant material behavior after complete strain reversal at σ_{maxC} (compression). Moreover, a slight localization of the maximum strain is observed, which is reproducible for each test. Furthermore, the location of maximum straining indicates the position, where necking occurs at strains higher than the uniform elongation ε_u. In case of miniaturized tensile tests of AZ31B, ε_u is determined to 0.093 ± 0.005 for 200 °C. The effect of a pre-strain above ε_u is seen in Fig. 5.

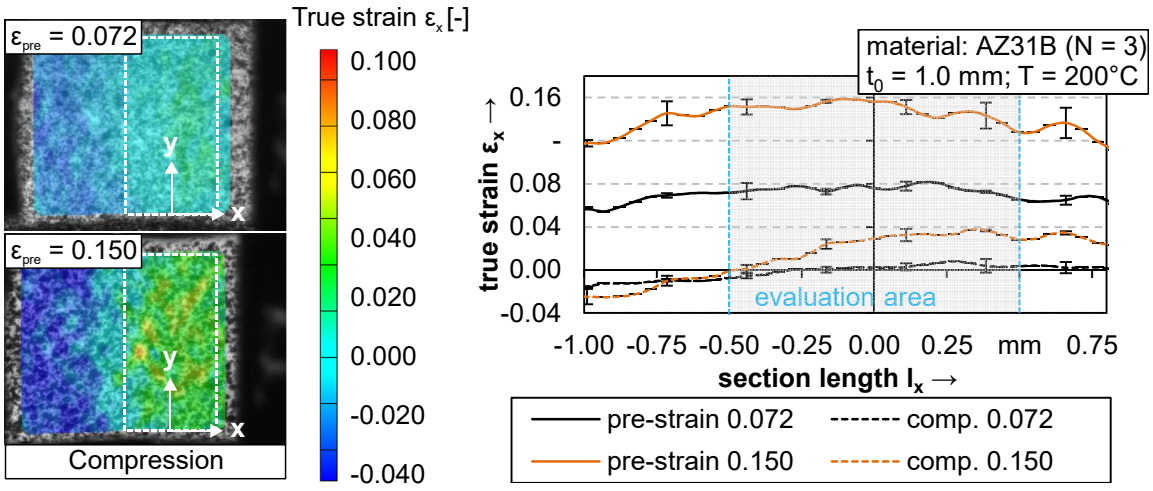

Fig. 5. Strain distribution during subsequent compressive loading of AZ31B at 200 °C

Concerning a pre-strain of 0.150, the pre-strain level exceeds the uniform elongation, where necking starts. Necking leads to a localization in the measuring area and an effect on the subsequent material behavior under compression as seen in Fig. 5. While the strain level for a pre-strain of

0.072 is almost recovered after compressive loading, the principal true strain ε_x vs. the section length l_x shows a significant inhomogeneity for a pre-strain of 0.150 (Fig. 5 right). In the results of the 2D strain distribution image (Fig. 5 left), the effect of pre-straining higher than the uniform elongation confirms a significant strain gradient under subsequent compressive loading. Hence, the identification of the isotropic-kinematic hardening behavior in the miniaturized tension-compression test of AZ31B is limited to a maximum average pre-strain level of 0.093 at an elevated temperature of 200 °C.

Kinematic Material Model Chaboche-Rousselier

As mentioned, the material behavior of AZ31B under cyclic loading shows a transient zone after load reversal, which needs to be mapped with a complex material model. Therefore, the kinematic model according to Chaboche and Rousselier [9] is identified. The model consists of a backstress tensor, which is composed of a summation of single exponential terms. Though, for the application of the transient zone, the model is reduced to two terms. For this reason, four independent material parameters C_1, r_1, C_2 and r_2 are identified and the deviation of the cyclic stress vs. strain curves to the experimental results is estimated (see Fig. 6). Besides, the isotropic hardening behavior is modeled with the hardening law Hockett-Sherby identified in the monotonic uniaxial tensile test.

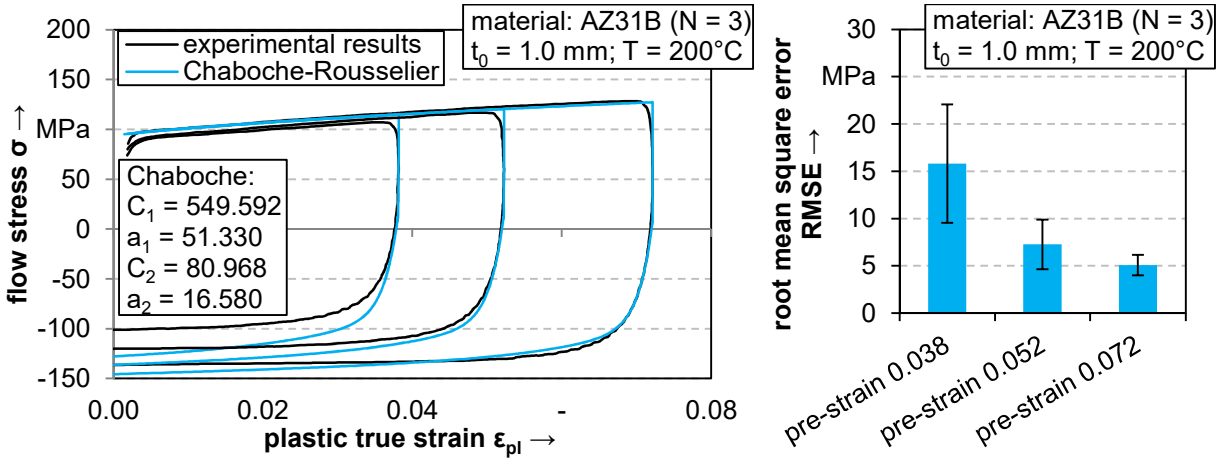

Fig. 6. Cyclic flow stress vs. plastic strain curves of AZ31B at 200 °C and identified Chaboche-Rousselier model – root mean square error (RMSE) of the identified model for the investigated pre-strains 0.038, 0.052 and 0.072

The root mean square error (RMSE) of the material model to the experimental cyclic flow stress vs. plastic strain curves is calculated. For the minimization of the residual, the RMSE value is determined as a sum of all investigated tests (N = 3) for all three pre-strain levels 0.038, 0.052 and 0.072. The results show a good accordance of the material model with the experiments in case of the two averaged pre-strain levels 0.052 and 0.072. This is also seen in case of the determined RMSE values, which are 7.272 ± 2.643 MPa for 0.052 and 5.061 ± 1.082 MPa for 0.072. However, the identified model significantly divers from the experimental results for a small pre-strain of 0.038. The deviation can also be seen for the RMSE value of 15.807 ± 6.254 MPa. Considering all levels of pre-strain in the identification procedure, the higher curvature of the flow stress vs. plastic strain curve for a small pre-strain of 0.038 cannot be mapped with the given material model without worsening the accuracy of the results at higher pre-strains.

During a forming operation, higher plastic strains occur. In favor, the material behavior at higher strains should preferably be taken into account in the present material model for an accurate numerical prediction of the forming process. To map the complete material behavior from smaller to higher pre-strains, a new material model is needed, e.g. to allow a change of the work-hardening exponent with increasing pre-strain.

Summary

A modified uniaxial tensile test setup for tension-compression tests of AZ31B sheets at an elevated temperature of 200 °C is presented. The temperature in the relevant area of the miniaturized tensile specimen is induced by conductive heating, while the temperature is detected and regulated with a pyrometer during testing. Local strains are detected by optical measurement. Since tension-compression tests are realized by pre-straining under tension with subsequent compressive loading, three different levels of pre-strain 0.038, 0.052 and 0.072 are analyzed. In addition, the influence of pre-straining higher than uniform elongation on the strain distribution is depicted. Cyclic stress vs. strain curves are determined, which exhibit an isotropic-kinematic hardening behavior with a transient zone of the yield stress during subsequent beginning of plastic yielding. Hence, the transient zone cannot be modeled with a single Bauschinger coefficient, the kinematic hardening law Chaboche-Rousselier is identified and the transferability to all investigated levels of pre-strain is examined with the help of the root mean square error (RMSE) analysis.

Acknowledgement

The authors are grateful to the German Research Foundation (DFG) for funding the research project "Contribution to an efficient FE-based design of magnesium sheet metal parts" (ME 2043/40-1).

References

[1] B. L. Mordike, T. Ebert, Magnesium Properties – applications – potential, Mater. Sci. Eng. A302 (2001) 37-45.

[2] J. Pflieger, M. Fischer, J. Stichling, P. Eyerer, Magnesium in Automotive Lightweight Design under Life Cycle Aspects, in: K. U. Kainer (Ed.), 6th Proc. Int. Conf. on Magnesium Alloys and Their Application, Weinheim, 2004, pp. 962-967.

[3] B.-A. Behrens, O. Vogt, Umformung von Magnesium, ke Komponenten + Systeme 12 (2005), 44.

[4] P. Juchmann, S. Wolff, New Perspectives with Magnesium Sheet, in: K. U. Kainer (Ed.), 6th Proc. Int. Conf. on Magnesium Alloys and Their Applications, Weinheim, 2004, pp. 1006-1012.

[5] M. Ullmann, F. Berge, K. Neh, R. Kawalla, H.-P. Vogt, Application of Magnesium Sheets and Strips in Vehicle Construction, R. Kawalla (Ed.), 4th AutoMetForm and 21st Sächsische Fachtagung für Umformtechnik (SFU), Freiberg, 2014, pp. 37-45.

[6] X.Y. Lou, M. Li, R. K. Boger, S. R. Agnew, R. H. Wagoner, Hardening evolution of AZ31B Mg Sheet, Int. J. Plasticity 23 (2007) 44-86.

[7] T. Hama, H. Nagao, Y. Kutchinomachi, H. Takuda, Effect of pre-strain on work-hardening behavior of magnesium alloy sheets upon cyclic loading, Mater. Sci. Eng. A 591 (2014), 69-77.

[8] A. Schaub, M. Lechner, M. Merklein, Druckversuch bei erhöhten Temperaturen, H. J. Christ (Ed.), Tagungsband Werkstoffprüfung DGM, Neu-Ulm, 2013, pp. 85-90.

[9] J. L. Chaboche, G. Rousselier, On the Plastic and Viscoplastic Constitutive Equations – Part I: Rules Developed With Internal Variable Concept, J. Press. Vess. Technol. 105 (1983) 153-158.

[10] J.-T. Gau, C. Principe, J. Wang, An experimental study on size effects on flow stress and formability of aluminm and brass for microforming, J. Mater. Process. Technol. 184 (2007) 42-46.